



UNIVERSITY OF LEEDS

This is a repository copy of *The synthesis of hydroxyapatite with different crystallinities by controlling the concentration of recombinant CEMP1 for biological application*.

White Rose Research Online URL for this paper:
<http://eprints.whiterose.ac.uk/92750/>

Version: Accepted Version

Article:

Chen, X, Liu, Y, Yang, J et al. (5 more authors) (2016) The synthesis of hydroxyapatite with different crystallinities by controlling the concentration of recombinant CEMP1 for biological application. *Materials Science and Engineering C*, 59. pp. 384-389. ISSN 0928-4931

<https://doi.org/10.1016/j.msec.2015.10.029>

© 2016. This manuscript version is made available under the CC-BY-NC-ND 4.0 license
<http://creativecommons.org/licenses/by-nc-nd/4.0/>

Reuse

Unless indicated otherwise, fulltext items are protected by copyright with all rights reserved. The copyright exception in section 29 of the Copyright, Designs and Patents Act 1988 allows the making of a single copy solely for the purpose of non-commercial research or private study within the limits of fair dealing. The publisher or other rights-holder may allow further reproduction and re-use of this version - refer to the White Rose Research Online record for this item. Where records identify the publisher as the copyright holder, users can verify any specific terms of use on the publisher's website.

Takedown

If you consider content in White Rose Research Online to be in breach of UK law, please notify us by emailing eprints@whiterose.ac.uk including the URL of the record and the reason for the withdrawal request.



eprints@whiterose.ac.uk
<https://eprints.whiterose.ac.uk/>

The synthesis of hydroxyapatite with different crystallinity by controlling the concentration of recombinant CEMP1 for biological application

Xiaofeng Chen¹, Yu Liu^{1#}, Jie Yang¹, Wenlei Wu¹, Leiyong Miao¹, Yijun Yu¹,
Xuebin Yang²,

Weibin Sun^{1#}

¹Hospital of Stomatology, Medical School of Nanjing University, Nanjing, Jiangsu 210093, People's Republic of China;

²Biomaterials and Tissue Engineering Group, Leeds Dental Institute, University of Leeds, United Kingdom.

#corresponding author

Name: Weibin Sun

Fax: +86 25 83620173.

E-mail : wbsun@nju.edu.cn

Address: Hospital of Stomatology, Medical School of Nanjing University, Nanjing, Jiangsu 210093, People's Republic of China

#corresponding author

Name: Yu liu

Fax: +86 25 83620173.

E-mail : lyvette@163.com

Address: Hospital of Stomatology, Medical School of Nanjing University, Nanjing, Jiangsu 210093, People's Republic of China

Abstract: Cementum protein 1 (CEMP1) has been reported to be cementum specific and it plays a role in the properties and structure of cementum mineralization. This study was carried out to test the hypothesis that, CEMP1 had the capacity to guide ordered HA formation as it accumulated at targeting site. Crystals induced by protein were prepared by biomimetic method. The effects of CEMP1 concentrations (0~100 $\mu\text{g/ml}$) on the rate of calcium phosphate precipitation was monitored during 48 hours, while the formed mineral phases were assessed utilizing transmission electron microscope (TEM), selected area electron diffraction (SAED), X-ray diffraction (XRD), and Fourier transform infrared spectroscopy (FTIR). The results showed that rhCEMP1 affected the crystal nucleation and growth. At lower rhCEMP1 concentrations (0~50 $\mu\text{g/ml}$), limited mineral formation occurred and only small bundles of HA crystals were found. However, with 100 $\mu\text{g/ml}$ of rhCEMP1, a predominance of organized linear needle-like HA crystals were observed. FTIR revealed the characteristic bands of HA appearing at 1106 cm^{-1} , 557 cm^{-1} , and 598 cm^{-1} . Therefore, increasing the concentration of rhCEMP1 can lead to the formation of ordered bundles of HA crystals in vitro.

Keywords: cementum protein 1; calcium phosphate; mineralization; crystal morphology

1. Introduction

Periodontitis is a major cause for tooth loss in adults. Periodontia reconstruction based on infection control is the key solution to periodontal treatment.

However, studies on Periodontia reconstruction have been hampered by the difficulties of cementum regeneration. Cementum represents a unique avascular mineralized connective tissue that covers the root surfaces of the teeth. It provides the interface through which the root surface is anchored to the collagen Sharpey's fibers of the periodontal ligament. Nevertheless, the complex processes that regulate cementogenesis and normal cementum metabolism remain unclear to date. Cementum is supposed to possess unique molecules which induce it to form a calcified tissue that differs from bone. Cementum protein 1 (CEMP1) is a cementum-specific marker. In vitro experiments showed that CEMP1 promoted cell attachment, differentiation, deposition rate, and affected the composition, and morphology of hydroxyapatite (HA) crystals formed by human cementoblast cells [1][2][3]. Since CEMP1 is synthesized by cementoblast cells and a restricted periodontal ligament cell subpopulation (cementoblast precursors), which suggests that this molecule is a cementum-specific biological marker and it may play a role as regulator of cell differentiation into a mineralizing cell phenotype [4]. Although the physiological function of CEMP1 is not completely understood, it is believed that this molecule plays an important role during the cementogenesis process and also as an inducer of the formation of mineralizing nodules and calcium deposition during the HA formation[5]. The process of mineralization in cementum is regulated and controlled spatially and temporarily by the extra-cellular macro-molecules synthesis by cementoblasts to form bio-composite structures [6]. These observations suggest that CEMP1 may play a regulatory role during the cementum formation and the bio-mineralization process.

The adsorption rate of protein is correlated oppositely with the HA crystallinity, that is, release kinetics of protein from HA depends on the crystallinity of HA. Amorphous calcium phosphate (ACP) had the highest release rate at 74%, whereas only 15% of proteins were released from the highly crystalline HA over 14-day [7]. ACP phases are one of the most frequent forms of CaP minerals in biological organisms [8]. In addition, ACP is found in several composite materials used in odontology as a remineralising phase for enamel and dentine, and its inclusion in toothpaste formulations as a remineralising agent for early carious lesions has been proposed. In the present study, we confirm that this protein promotes HA crystal nucleation in vitro through a concentration dependent manner. We anticipate that these studies will improve the knowledge of the relationship between recombinant protein and the crystalline of calcium phosphate and lead to the development of novel protein loading calcium phosphate material for dental tissue repair and regeneration.

2. Materials and methods

2.1. Expression and purification of CEMP1

The open reading frame of CEMP1 was obtained from PubMed (GenBank Accession No. NP_001041677), the protein coding sequence was optimized by Codon Adaptation Tool (<http://www.jcat.de/>). The optimized coding sequence was synthesized (Invitrogen) and then subcloned into the pENTR/SD/D vector (Invitrogen) and the resultant pENTR/SD/D-CEMP1 cDNA construct ligated into a pET-28a (+) vector pET-28a-CEMP1. Then the plasmid was sequenced ligated into a pET-28a (+) vector pET-28a-CEMP1. Then the plasmid was sequenced to confirm the insertion of CEMP1. The plasmid was introduced into BL21 (DE3) expression host Escherichia coli strain (Invitrogen). E. coli BL21 (DE3) containing pET-28a-CEMP1 construction was grown at 37 °C in Luria-Bertani medium containing 100 µg/ml kanamycin to an O.D. of 0.4 at 600 nm. Then IPTG (isopropyl β-D-thiogalactoside) was added to a final concentration of 1mM and continued to be grown at

28 °C for 3 h. Recombinant human CEMP1 protein collected from conditioned media was purified by Ni-NTA His•Bind[®] Resin (Novagen). Determination of protein purity was performed by 12% SDS-PAGE and Western blotting.

2.2. Western blot analysis

Recombinant human CEMP1 (10 µg) was separated by 12% SDS-PAGE and electroblotted onto Immobilon-P (PVDF) nitrocellulose membrane (Millipore). Anti-rhCEMP1 polyclonal antibody was used to specifically identify the CEMP1 gene product. Peroxidase-conjugated goat anti-rabbit IgG was used as secondary antibody and detection was performed.

2.3. Cell culture

Human periodontal ligament cells (PDLC) were retrieved using a previously described method with some modifications [9]. PDLCs were isolated from normal premolar extracted for orthodontic reasons from 5 individuals aged 16~18 years. All procedures followed the approved ethical guidelines set by the Ethics Committee of Nanjing Stomatological Hospital. Briefly, intact teeth were collected from individuals undergoing orthodontic treatment. Teeth were rinsed three times with phosphate-buffered saline (PBS) supplemented with antibiotics (streptomycin 100 µg/ml, penicillin 100 units/ml). Periodontal ligament tissue in the middle-third of the root was scraped from the root surface with a surgical scalpel. Cell cultures were maintained in an atmosphere of 95% air/5% CO₂ at 37 °C with 100% humidity. Cells were expanded and grown in DMEM (Dulbecco's modified Eagle's medium) supplemented with 10% FBS (fetal bovine serum), and antibiotics (streptomycin 100 mg/ml, penicillin 100 units/ml). Cells at the third passage were used for the experiments.

To evaluate whether CEMP1 produced in *E. coli* had same effect as cementum extract, human PDLCs were suspended to 5×10^5 /ml and planted into 12 wells plate for 24 h at 37 °C. Then they were maintained in either experimental (0.25 µg/ml of rhCEMP1) or control media (0 µg/ml of rhCEMP1) for 48 h.

2.4. Real-time polymerase chain reaction (PCR) analysis

Total RNA was prepared from cells using the RNAeasy Mini Kit according to the manufacturer instructions (Qiagen). One microgram of total RNA was used for complementary DNA (cDNA) synthesis using a PrimeScript™ II 1st Strand cDNA Synthesis Kit for RT-PCR (Takara). Quantitative real-time PCR was carried out using Universal SYBR Green Supermix (Bio-Rad). Primer sequences of human β-actin and CEMP1 were as follows: β-actin, Forward 5'-GATGAGATTGGCATGGCTT-3' and Reverse 5'-CACCTTCACCGTTCCAGTTTT-3'; CEMP1, Forward 5'-GGCGATGCTCAACCTCTAAC-3' and Reverse 5'-GATACCCACCTCTGCCTTGA-3'. Amplification conditions were 95 °C for 10 min for denaturation, then 40 cycles of 95 °C for 15 s, 60 °C for 1 min and 95 °C for 15 s followed by a melting curve from 58 to 98 °C. Reaction products were quantified using StepOne Software Version 2.1. Expression level values were normalized to that of an internal control, β-actin.

Statistical analysis. Data were analyzed using Student's t test. Data were collected from at least three independent experiments. $P < 0.05$ was considered statistically significant. Statistical analyses were performed with SPSS Version. 19.0.

2.5. Mineralization experiments

Preparation of samples. Lyophilized rhCEMP1 were dissolved in distilled deionized water (DDW) to give a concentration of 2 mg/ml. Dynamic light scattering was utilized to ensure complete dissolution of protein samples [10]. Protein stock solutions were centrifuged

(11 340×g, Eppendorf Centrifuge 5403) at 4 °C for 20 min, just prior to use to remove dust and any particulate matter. Aliquots of 100 mM stock solutions of CaCl₂ (Sigma, >99.0% pure) and (NH₄)₂HPO₄ (Sigma, >99.0% pure) were then added to the samples to yield final concentrations of 2.5 mM Ca²⁺, 1.5 mM P and 25~100 μg/ml protein, with a final volume of 100 ml. All solutions (except protein solutions) were filtered (0.22-μm Isopore filters, Millipore) before use. The solutions were adjusted to pH 8.0 with 2N NH₄OH at 4 °C. The sample was then transferred into a 37 °C incubator for 48 h. To minimize evaporation, the reaction tube was tightly sealed Parafilm (America National Can). After 2 days of reaction, the precipitates were washed three times with deionized water. The precipitates were finally dried using a VirTis freeze drier. Control experiments were performed similarly without the addition of rhCEMP1. Experiments were repeated 3 times.

TEM analyses of mineral products. 30 μl aliquots were placed on carbon-coated Ni grids for 1min, and then quickly rinsed with distilled water, blotted against filter paper, and air dried. The samples were examined by transmission electron microscope (TEM) in bright field and selected area diffraction (SAED) modes. The images and diffraction patterns were captured using CCD (AMT) and/or still cameras. The average diameter of mineralization deposit was measured by counting 200 crystals from 5 TEM micrographs with Nano Measurer Version. 1.2. [11].

XRD examinations were made with freeze-dried samples with Philips diffractometer ((X'Pert Pro, Philips, Almelo, The Netherlands) using CuKα in the wide range of Bragg's angles 20° < 2θ < 60° at room temperature. Scan rate was 2°/min [12].

Fourier Transform-Infrared Spectroscopic Analyses. Samples were placed on a KBr IR Card (International Crystal Labs, Garfield, N.J., USA), and air-dried. The Fourier

transform-infrared (FTIR) spectra ($4,000-450\text{ cm}^{-1}$) of samples were recorded using a Multiscope FTIR microscope (Perkin-Elmer) as reported [13].

3. Results and Discussions

3.1. Characterization of the rhCEMP1 protein.

pET-28a-CEMP1 was confirmed by restriction enzymes digestion and sequencing (Fig.1). A band of about 750 bp representing CEMP1 was evident (Fig.1A). Analysis of the sequencing indicated CEMP1 was rightly inserted into the plasmid (Fig.1B). In order to characterize the protein and produce an anti-CEMP1 antibody, the protein was expressed in *E.coli* and analyzed using SDS-PAGE (Fig. 2 lane 1-3). When the protein was purified using Ni²⁺ affinity chromatography, a major band of approximately 36 kDa was seen (Fig. 2, lane 2). The molecular weight of the predicted size is 25.9 kDa. The difference in molecular weight of the predicted size and this band is due to the presence of the polyhistidine tag which adds 10 kDa to the molecular weight showed in SDS-PAGE [14]. Antibody specific for anti-CEMP1 recognized a 36 kDa band, confirming the identity of this protein as rhCEMP1 (Fig. 2, lane 3) . These results were in accordance with those researches expressing rhCEMP1 in a prokaryotic expression system [15]. Westerns blots using protein extracts obtained from cementoblastoma and periodontal ligament cells with the CEMP1 antibody showed a main protein band with Mr 44,000 and an additional cementoblastoma protein species of Mr 56000 and Mr 26,000 [16]. The relationship of these three species is not clear. It is still unknown whether the variation is caused by posttranslational modifications of removal of peptides or modification of amino acids. There is no sufficient evidence to show the difference of their effects on cell differentiation and mineralization.

3.2. The effect of rhCEMP1 on periodontal ligament cell CEMP1 mRNA expression.

To examine whether rhCEMP1 expressed in a prokaryotic expression system had the same cell interaction with that of a eukaryotic one, we measured the expression of *cemp1* mRNA after rhCEMP1 induction. The result showed in Fig. 3 indicated that *cemp1* mRNA was expressed in both control and experimental PDLCs at 48 h of culture. The expression of *cemp1* was observed in the experimental culture (0.25 µg/ml rhCEMP1) was about 3 folds as much as the control culture (0 µg/ml rhCEMP1). PDLCs have been reported to have the potential to differentiate into cementoblasts [17]. The overexpression of *cemp1* induces a cementoblastic phenotype and reduces osteoblastic differentiation in PDLCs. CEMP1 is not only a marker protein for cementoblasts-related cells, but also regulates cementoblast commitment in PDLCs [18]. Polymerase chain reaction analysis of ALP, bone sialoprotein, osteocalcin and cementum attachment protein show that overexpression of CEMP1 enhances these cementogenic potential relative genes' expression [19][20][21].

3.3. rhCEMP1 effect on apatite formation.

The morphology of apatite crystals grown in different situations were characterized by TEM as shown in Fig. 4. All of the obtained crystals had a ribbon-like shape. Based on the electron diffraction analysis, the mineral phase was either HA or octacalcium phosphate (OCP). The morphological disposition of the HA crystals formed in the presence of various concentration of rhCEMP1 had same trend. Randomly arranged HA crystals (Fig.4A) show an average size of 85 nm (E). Well-aligned Bundles of HA crystals were formed with the participation of rhCEMP1 (Fig.4B-C). (Fig.4D) indicates the presence of bundles of well-oriented HA crystals with an average size of 207 nm (Fig.4F). The morphologies and aspect ratios of HA particles under different reaction conditions were shown in Fig. 4. As revealed in Fig. 4, controlling the concentration of rhCEMP1 could give rise to varied morphologies and aspect ratios of the HA particles. The aspect ratios of the HA particles were 2.68 ± 0.72

(Fig. 4A), 4.40 ± 0.75 (Fig. 4B), 4.76 ± 1.39 (Fig. 4C) and 5.50 ± 1.23 (Fig. 4D) when the concentration of rhCEMP1 varied from 0, 25, 50 to 100 $\mu\text{g/ml}$, respectively. The crystal was ribbon-like without the presence of rhCEMP1 (Fig. 4A) and then it obtain a needle-like shape under the induction of rhCEMP1 with an increase in aspect ratio (Fig. 4B-C). The TEM results suggested that rhCEMP1 assembly played a role in organizing calcium phosphate crystals into parallel arrays, whereas its hydrophobic core was responsible for the regulation of crystal growth. It was feasible that this C-terminal domain was involved in the regulation of rhCEMP1 assembly, which in turn affected the organization and shape of the growing crystals, through protein-protein and protein-crystal interactions [22].

Selected area electron diffraction (SAED) analyses of the mineral phases formed in the presence of various concentration of rhCEMP1 were shown in Fig. 5. SAED pattern of HA formed without rhCEMP1 shows concentric ring-like pattern suggesting polycrystalline nature (Fig. 5A). The discrete diffraction spots and the rings seen in Fig. 5B are consistent with randomly arranged HA crystals. The presence of higher number of electron diffraction spots and absence of well-separated concentric rings at its background in (Fig. 5C) indicates the presence of bundles of well-oriented HA crystals. From this data, we can assume that rhCEMP1 regulate an oriented HA growth.

The XRD patterns of the mineralization deposits are shown in Fig. 6. The diffraction patterns are similar with those of standard HA sample (JCPDS No. 09-0432). The peaks at 31.76° , and 32.12° corresponded to the expected HA peaks at the 211 and 112 planes, respectively, thereby confirming that the precipitates were HA crystals. The peaks ascribed to the 211, 122 planes were not completely separated, suggesting that the HA precipitates were low in crystallinity.. The crystallinity of 211 and 300 plane of HA prepared with more rhCEMP1 addition increased. Particularly, the diffraction peak of 211 was the greatest.

Fig. 7 represents the FTIR spectra of the samples generated in the solutions with concentration of rhCEMP1 ranging from 0 to 100 $\mu\text{g/ml}$ for 48 h. The broadband at 3464 cm^{-1} was assigned to the stretching vibration of lattice hydroxyl (-OH) groups [23]. The characteristic sharp bands of HA, which appeared in the regions of 1106 cm^{-1} , cm^{-1} , 598 and 557 cm^{-1} in spectra of HA, were assigned to the regular tetrahedral (PO_4^{3-}), P-O stretching, and O-P-O bending vibrations, respectively (please see Fig. 7A) [24]. These bands are present at their characteristic positions in the spectra of rhCEMP1 50 and 100 $\mu\text{g/ml}$. The bands observed in HA at 1384 cm^{-1} are due to the stretching vibration of carbonate [25][26]. The appearance of absorption bands at 1463 and 865 cm^{-1} indicated the occupation of CO_3^{2-} ions onto and/or OH^- ions [27]. When rhCEMP1 was added to reaction system, chemical changes were observed in the IR spectra at 1624 and 1668 cm^{-1} . This can be ascribed to the amide I band that represents the stretching vibrations of C=O bonds in the backbone of the protein (Fig. 7B and C). Protein structure has been examined with bands denoted as amide I (centered at 1650 cm^{-1}), amide II (centered at 1550 cm^{-1}) and amide III (centered at 1250 cm^{-1}). In the amide I region, IR bands in the 695~1660 cm^{-1} are assigned to beta sheet, 1660~1650 cm^{-1} to the alpha-helix structure, 1650~1640 cm^{-1} to random structure, and 1640~1620 to beta-sheet and turn structure [28].

Characteristics of the protein, such as phosphorylated variant, polar and charged amino acids and self-assembly, seem to be mainly responsible for its inhibitory or stimulative effect in mineralization. The N-terminus of the phosphorylated variant is found to be consistently closer to the HA surface than the non-phosphorylated variant [29]. Researchers find that the negatively charged ones, such as glutamic acid (Glu) and phosphoserine (P-Ser) seem to be mainly responsible for the inhibitory effect in mineralization. There is a strong inhibitory effect of arginine (Arg) on HA nucleation [30]. rhCEMP1 contained both positively and negatively charged residues with a proportion of

26/247 and 14/247 respectively. The arrangement of these charges on the protein, as well as the complementarities between the charged groups on the protein and the growing apatite surfaces, may influence the crystal growth behavior and also lead to more cohesive cements for higher rhCEMP1 contents. In this study, rhCEMP1 aggregates may adopt a functional role which facilitates the nucleation, growth and direction of HA crystals. Protein self-assembles into nanospheres which then form aggregates resembling nanostrings [31]. By this way, the self-assembly of this protein suggests the formation of functional building blocks that can facilitate oriented HA crystal formation by providing the ultrastructural framework.

Although the critical protein concentration needed may be depended on other solution factors (e.g. Mineral ion levels, pH, ionic, temperature), present results clearly show that an increase in the concentration of rhCEMP1 can result in appropriate kinetic conditions that lead to the formation of ordered bundles of HA crystals in vitro. However, concentration less than 200 $\mu\text{g/ml}$ was too low for other proteins such as amelogenins that the influence of hydrophilic C-terminus was lost [32]. The HA with variable chemical substitutions has been considered as the major component in the mineralized tissues. Various metastable crystalline phases have been suggested as transitory precursors of HA, there seems to be a rule for the nature of these phases and their temporal evolution [33]. Dicalcium phosphate dihydrate (DCPD) and OCP like phases are likely to occur on the course of osteoblast mineralization, and the mineral-associated proteins might be involved in modulating the mineral phase transformation. The time depended phase shift was not included in the study while our data (not shown) suggested that 48 hours was the minimum time to discover crystallinity variance between distinct concentrations. In the future, we will further characterize this protein and confirm whether self-assembly, phosphorylation and pH value of the solution play a role in the mineralization.

5. Conclusions

Studies on periodontal regeneration have been hampered by the failure of cementum induction. CEMP1 may be the most important molecule in cementogenesis that makes cementum differ from other hard tissues. Our data confirm that rhCEMP1 produced in a prokaryotic system has the similar functions with CEMP1 from a eukaryotic system. The rhCEMP1 in this study can regulate cementum specific gene expression in PDLC. It also proved that rhCEMP1-mediated mineralization process was concentration dependent. Moreover, this kind of recombinant protein-loading HA with different crystallinity lead to the development of new protein loading calcium phosphate material for dental tissue repair and regeneration.

6. Acknowledgments and declaration of interest

The authors thank Prof. Yi-nong Lv (Nanjing University of Technology and Lin-fei Ding (Nanjing Agricultural University) for their cooperation and valuable discussion. This study was supported by funds from National Natural Science Foundation of China (No: 81271155, No: 81300852), Jiangsu Province Natural Science Foundation of China (BK20130079). The authors report no conflicts of interest.

References

- [1] H. Arzate, J. Chimal-Monroy, L. Hernandez-Lagunas, L. Diaz de Leon, Human cementum protein extract promotes chondrogenesis and mineralization in mesenchymal cells, *Journal of periodontal research*, 31 (1996) 144-148.
- [2] M.A. Alvarez Perez, S. Pitaru, O. Alvarez Fregoso, J. Reyes Gasga, H. Arzate, Anti-cementoblastoma-derived protein antibody partially inhibits mineralization on a cementoblastic cell line, *Journal of structural biology*, 143 (2003) 1-13.

[3] B. Carmona-Rodriguez, M.A. Alvarez-Perez, A.S. Narayanan, M. Zeichner-David, J. Reyes-Gasga, J. Molina-Guarneros, A.L. Garcia-Hernandez, J.L. Suarez-Franco, I.G. Chavarria, E. Villarreal-Ramirez, H. Arzate, Human Cementum Protein 1 induces expression of bone and cementum proteins by human gingival fibroblasts, *Biochemical and biophysical research communications*, 358 (2007) 763-769.

[4] M.A. Alvarez-Perez, S. Narayanan, M. Zeichner-David, B. Rodriguez Carmona, H. Arzate, Molecular cloning, expression and immunolocalization of a novel human cementum-derived protein (CP-23), *Bone*, 38 (2006) 409-419.

[5] E. Villarreal-Ramirez, A. Moreno, J. Mas-Oliva, J.L. Chavez-Pacheco, A.S. Narayanan, I. Gil-Chavarria, M. Zeichner-David, H. Arzate, Characterization of recombinant human cementum protein 1 (hrCEMP1): Primary role in biomineralization, *Biochemical and biophysical research communications*, 384 (2009) 49-54.

[6] M.D. Grynpas, S. Omelon, *Bone*, 41 (2007) 162-164. M.D. Grynpas, S. Omelon, Transient precursor strategy or very small biological apatite crystals?, *Bone*, 41 (2007) 162-164.

[7] W.H. Lee, A.V. Zavgorodniy, C.Y. Loo, R. Rohanizadeh, Synthesis and characterization of hydroxyapatite with different crystallinity: effects on protein adsorption and release, *Journal of biomedical materials research. Part A*, 100 (2012) 1539-1549.

[8] E.D. Eanes, Amorphous calcium phosphate: thermodynamic and kinetic considerations, *Journal of dental research*, 77 (1998) 6-7.

[9] K. Tanaka, K. Iwasaki, K.E. Feghali, M. Komaki, I. Ishikawa, Y. Izumi, Comparison of characteristics of periodontal ligament cells obtained from outgrowth and enzyme-digested culture methods, *Archives of oral biology*, 56 (2011) 380-388.

[10] F.B. Wiedemann-Bidlack, E. Beniash, Y. Yamakoshi, J.P. Simmer, H.C. Margolis, pH triggered self-assembly of native and recombinant amelogenins under physiological pH and temperature in vitro, *Journal of structural biology*, 160 (2007) 57-69.

[11] F.B. Wiedemann-Bidlack, S.Y. Kwak, E. Beniash, Y. Yamakoshi, J.P. Simmer, H.C. Margolis, Effects of phosphorylation on the self-assembly of native full-length porcine amelogenin and its regulation of calcium phosphate formation in vitro, *Journal of structural biology*, 173 (2011) 250-260.

[12] P. Singh, R.C. YashRoy, M. Hoque, Augmented bone-matrix formation and osteogenesis under magnetic field stimulation in vivo XRD, TEM and SEM investigations, *Indian journal of biochemistry & biophysics*, 43 (2006) 167-172.

[13] E. Le Norcy, S.Y. Kwak, F.B. Wiedemann-Bidlack, E. Beniash, Y. Yamakoshi, J.P. Simmer, H.C. Margolis, Potential role of the amelogenin N-terminus in the regulation of calcium phosphate formation in vitro, *Cells, tissues, organs*, 194 (2011) 188-193.

[14] I. Navarro-Gonzalez, S.F. Alvaro, G.C. Francisco, Overexpression, purification, and biochemical characterization of the esterase Est0796 from *Lactobacillus plantarum* WCFS1, *Molecular biotechnology*, 54 (2013) 651-660.

[15] L. Hoz, E. Romo, M. Zeichner-David, M. Sanz, J. Nunez, L. Gaitan, G. Mercado, H. Arzate, Cementum protein 1 (CEMP1) induces differentiation by human periodontal ligament cells under three-dimensional culture conditions, *Cell biology international*, 36 (2012) 129-136.

[16] M. A. Alvarez-Perez, S. Narayanan, M. Zeichner-David, B. R.Carmona, H.Arzate, Molecular cloning, expression and immunolocalization of a novel human cementum-derived protein (CP-23), *Bone*. 38(2006.) 409-19.

[17] S. Fujii, H. Maeda, N. Wada, A. Tomokiyo, M. Saito, A. Akamine, Investigating a clonal human periodontal ligament progenitor/stem cell line in vitro and in vivo, *Journal of cellular physiology*, 215 (2008) 743-749.

[18] M. Komaki, K. Iwasaki, H. Arzate, A.S. Narayanan, Y. Izumi, I. Morita, Cementum Protein 1 (CEMP1) Induces a Cementoblastic Phenotype and Reduces Osteoblastic Differentiation in Periodontal Ligament Cells, *Journal of cellular physiology*, 227 (2012) 649-657.

[19] I.C. Gay, S. Chen, M. MacDougall, Isolation and characterization of multipotent human periodontal ligament stem cells, *Orthodontics & craniofacial research*, 10 (2007) 149-160.

[20] M.G. Flores, M. Hasegawa, M. Yamato, R. Takagi, T. Okano, I. Ishikawa, Cementum-periodontal ligament complex regeneration using the cell sheet technique, *Journal of periodontal research*, 43 (2008) 364-371.

[21] A. Tomokiyo, H. Maeda, S. Fujii, N. Wada, K. Shima, A. Akamine, Development of a multipotent clonal human periodontal ligament cell line, *Differentiation; research in biological diversity*, 76 (2008) 337-347.

[22] E. Beniash, J.P. Simmer, H.C. Margolis, The effect of recombinant mouse amelogenins on the formation and organization of hydroxyapatite crystals in vitro, *Journal of structural biology*, 149 (2005) 182-190.

[23] Y. Pekounov, K. Chakarova, K. Hadjiivanov, Surface acidity of calcium phosphate and calcium hydroxyapatite: FTIR spectroscopic study of low-temperature CO adsorption, *Mater. Sci. Eng. C*, 29 (2009) 1178-1181.

[24] D.Q. Wei, Y. Zhou, D.C. Jia, Y.M. Wang, Characteristic and in vitro bioactivity of a micro-arc-oxidized TiO₂-based coating after chemical treatment, *Acta Biomaterialia*, 3 (2007), pp. 817–827.

[25] I. Demnati, D. Grossin, C. Combes, M. Parco, I. Braceras, C. Rey, A comparative physico-chemical study of chlorapatite and hydroxyapatite: from powders to plasma sprayed thin coatings, *Biomedical materials*, 7 (2012) 054101.

[26] P.N. Kumta, C. Sfeir, D.H. Lee, D. Olton, D. Choi, An alternative chemical route for the synthesis and thermal stability of chemically enriched hydroxyapatite, *Acta biomaterialia*, 1 (2005) 65-83.

[27] B. Jokic, M. Mitric, V. Radmilovic, S. Drmanic, R. Petrovic, D. Janackovic, Synthesis and characterization of monetite and hydroxyapatite whiskers obtained by a hydrothermal method, *Ceramics International* Jan 37(2011) 167–173.

[28] J. Xie, C. Riley, M. Kumar, K. Chittur, FTIR/ATR study of protein adsorption and brushite transformation to hydroxyapatite, *Biomaterials*, 23 (2002) 3609-3616.

[29] D.L. Masica, J.J. Gray, W.J. Shaw, The journal of physical chemistry. C, Partial high-resolution structure of phosphorylated and non-phosphorylated leucine-rich amelogenin protein adsorbed to hydroxyapatite, *Nanomaterials and interfaces*, 115 (2011) 13775-13785.

[30] M.T. Jahromi, G. Yao, M. Cerruti, The importance of amino acid interactions in the crystallization of hydroxyapatite, *Journal of the Royal Society, Interface / the Royal Society*, 10 (2013) 20120906.

[31] G. Montoya, J. Arenas, E. Romo, M. Zeichner-David, M. Alvarez, A.S. Narayanan, U. Velazquez, G. Mercado, H. Arzate, Human recombinant cementum attachment protein (hrPTPLa/CAP) promotes hydroxyapatite crystal formation in vitro and bone healing in vivo, *Bone*, 69 (2014) 154-164.

[32] S.Y. Kwak, S. Kim, Y. Yamakoshi, J.P. Simmer, E. Beniash, H.C. Margolis, Regulation of calcium

phosphate formation by native amelogenins in vitro, *Connective tissue research*, 55 Suppl 1 (2014) 21-24.

[33] Z.L. Zhang, X.R. Chen, S. Bian, J. Huang, T.L. Zhang, K. Wang, Identification of dicalcium phosphate dihydrate deposited during osteoblast mineralization in vitro, *Journal of inorganic biochemistry*, 131 (2014) 09-114.

Figure Caption

Fig. 1 Affirmation of pET-28a-CEMP1. (A) Affirmation of the pET-28a-CEMP1 with restriction enzymes digestion. (B) Affirmation of CEMP1 insertion into pET-28a vector by sequencing.

Fig. 2 SDS-PAGE and Western blot of rhCEMP1. Protein Marker ranges from 26 to 172 kDa (lane M). Coomassie blue-stained gel of 1.0 mM IPTG induced cultures grown for 3 h (lane 1). Ni²⁺ affinity chromatograph of rhCEMP1. The purified protein band represents a 36 kDa species (lane 2). Western blots of the rhCEMP1 gene product with anti-CEMP1 antibody (lane 3). Arrow indicates the 36 kDa band of rhCEMP1.

Fig. 3 Quantitative real-time PCR analysis for rhCEMP1 on PDLCs CEMP1 mRNA expression. Cells were treated without (0 µg/ml) or with (0.25 µg/ml) rhCEMP1 for 48 h. Asterisk indicated statistical significance *P<0.05.

Fig. 4 TEM analyses of morphological disposition of the hydroxyapatite crystals formed in the presence of various concentration of rhCEMP1; (A) in the absence of protein (control), (B) 25 $\mu\text{g/ml}$, (C) 50 $\mu\text{g/ml}$, and (D) 100 $\mu\text{g/ml}$. Randomly arranged hydroxyapatite (HA) crystals (A) show an average size of 85 nm (E). Well-aligned Bundles of HA crystals were formed with the participation of rhCEMP1 (B, C, D) indicates the presence of bundles of well-oriented HA crystals. These structures show an average size of 207 nm (F).

Fig. 5 Selected area electron diffraction (SAED) analyses of mineral phases formed in the presence of various concentration of rhCEMP1; (A) in the absence of protein (control), (B) 25 $\mu\text{g/ml}$, (C) 50 $\mu\text{g/ml}$, and (D) 100 $\mu\text{g/ml}$. The discrete diffraction spots and sharp rings seen in (A) and (B) are consistent with randomly arranged hydroxyapatite (HA) crystals while the presence of narrow diffraction arcs in (C) indicates the presence of bundles of well-oriented HA crystals.

Fig. 6 Effect of rhCEMP1 concentration on X-ray diffraction (XRD) patterns of mineral products formed in different concentrations of rhCEMP1 (0, 50, 100 $\mu\text{g/ml}$). The vertical lines are the reference pattern of HA (PDF #26-1056).

Fig. 7 Fourier transform infrared spectroscopy (FTIR) of mineral products formed in different concentrations of rhCEMP1 (0~100 $\mu\text{g/ml}$).

Figure 1

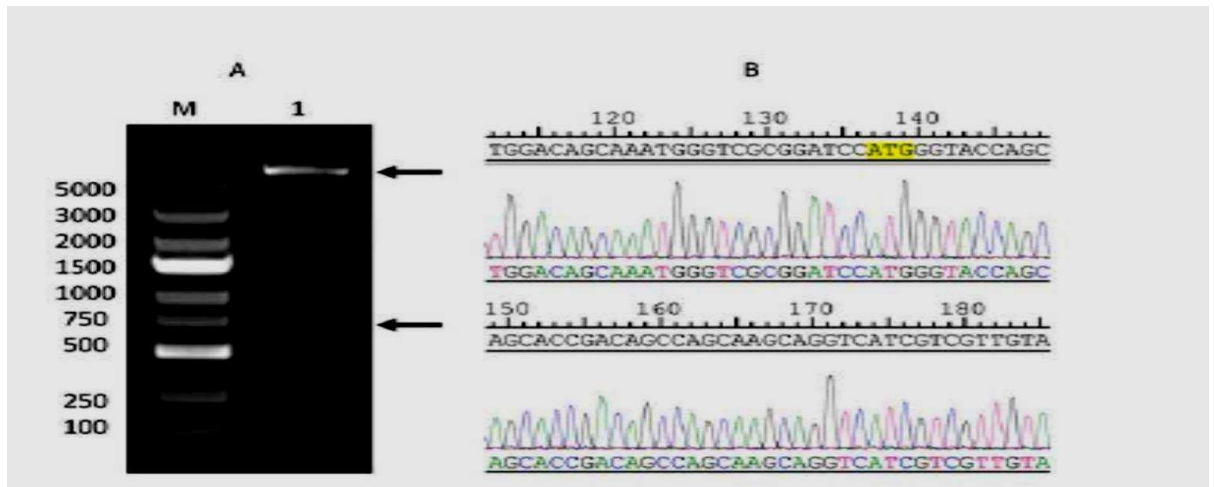


Figure 2

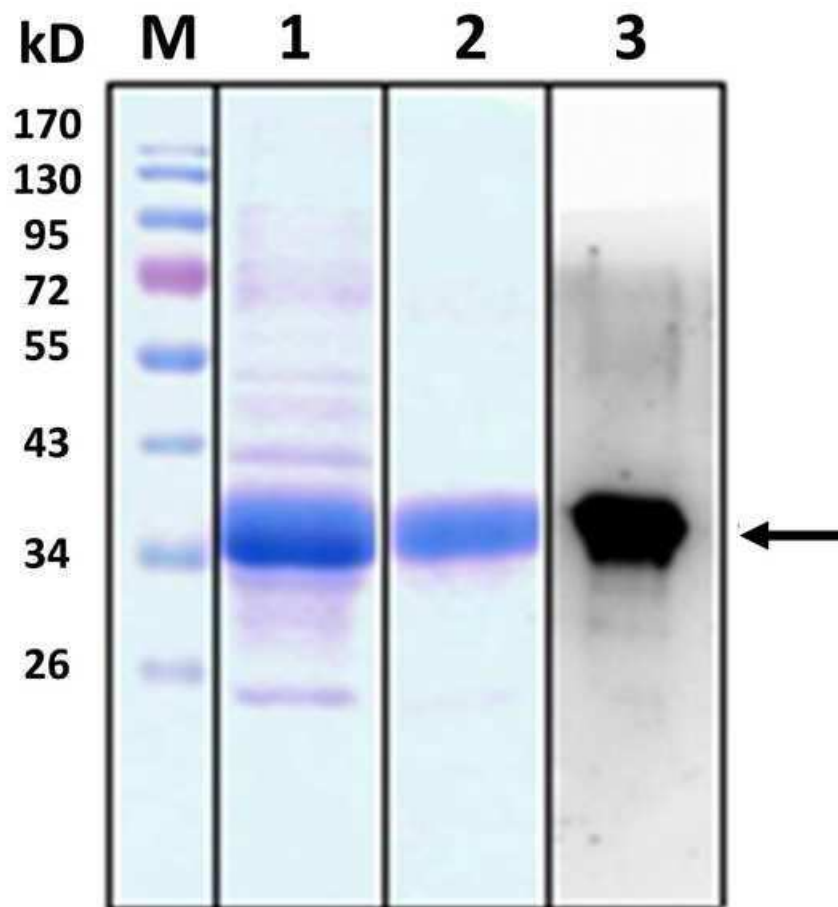


Figure 3

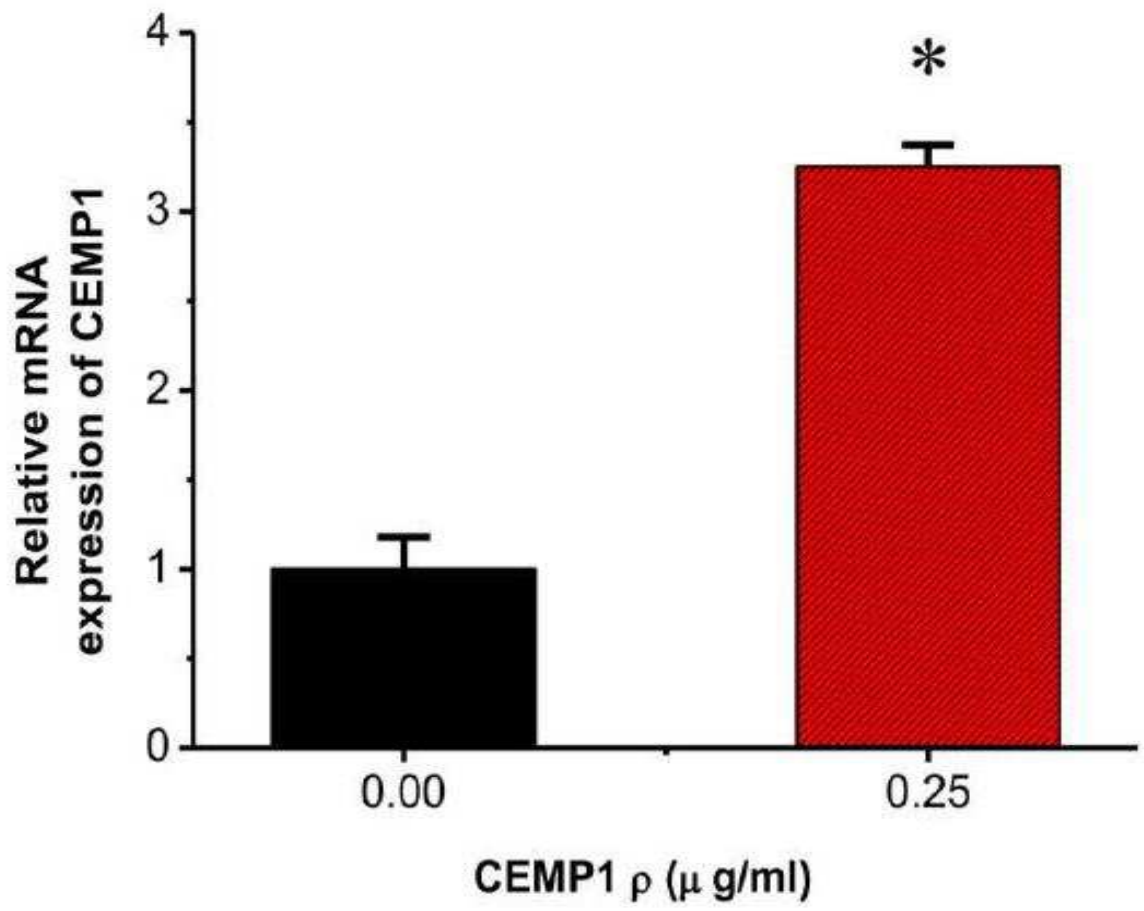


Figure 4

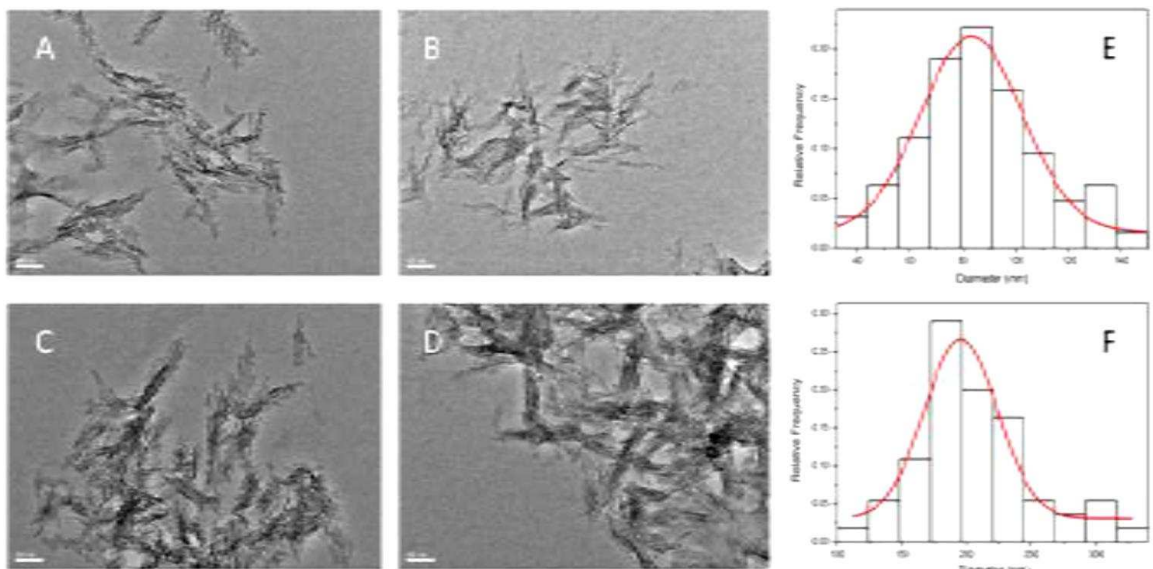


Figure 5

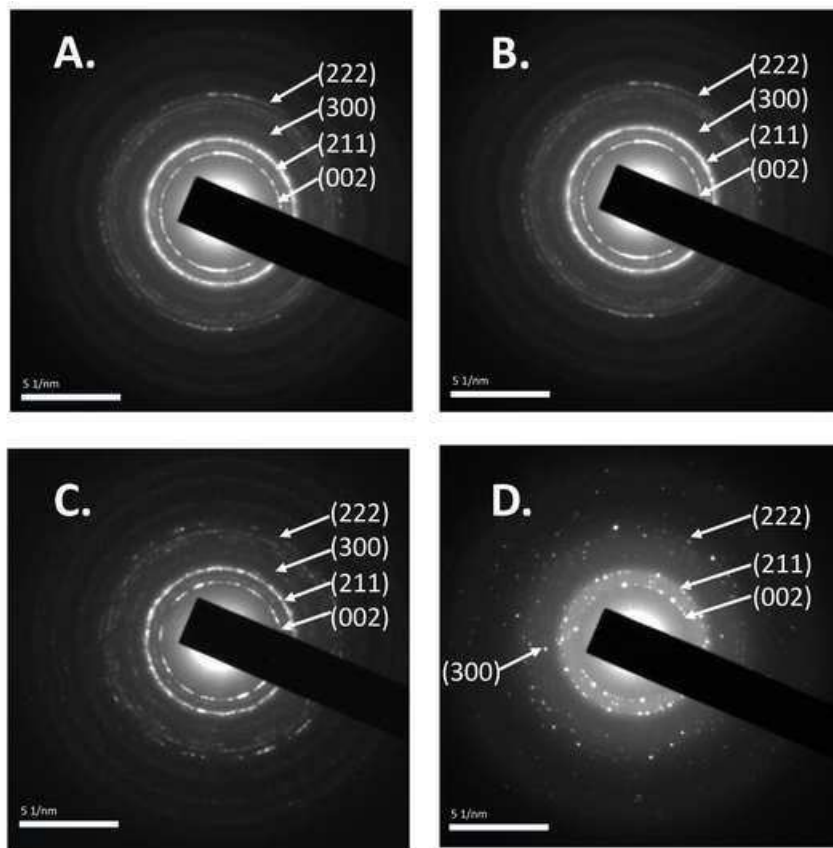


Figure 6

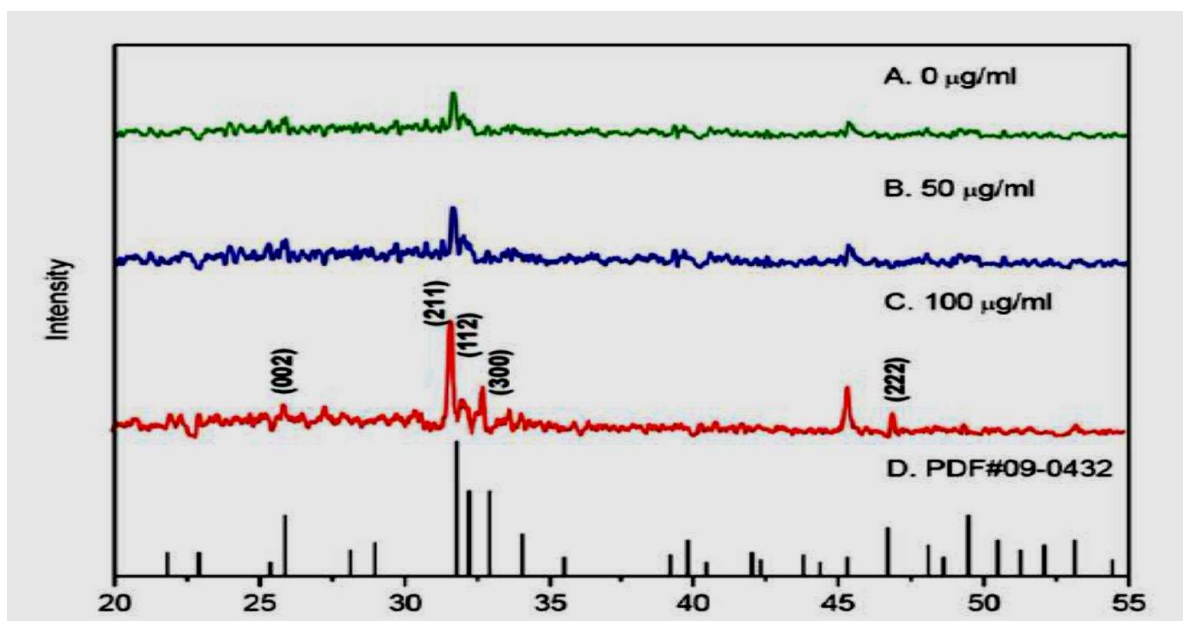


Figure 7

